The evaporation efficiency of a passive capillary irrigated green roof system: a case study in Amsterdam, the Netherlands.

Abstract: Green roofs are promoted as a climate adaptation measure to lower air temperatures and improve comfort in urban areas, especially during intensive dry and warm spells. However, there is much debate on the effectiveness of this measure. The cooling effect of a green roof is directly related to evapotranspiration and therefore to the availability of water in the system. When water runs short, evapotranspiration will decrease and the cooling effect might become negligible. To gain insight in the effect of water availability on evapotranspiration and the energy balance, we compared the actual evaporation rate and latent heat flux of a conventional green roof with that of so called blue-green roofs equipped with a passive capillary irrigation system. With on-site climatic measurements, the potential evaporation was determined by parameterizing the Penman-Monteith equation. The potential evaporation was afterwards compared with the actual evaporation of weighing lysimeters to evaluate the efficiency of the different roofs. Also, climatic data from the "The Royal Netherlands Meteorological Institute" (KNMI) was used to determine the hydrological behaviour of the green roof for an extended period. The blue-green roofs have a larger evaporation efficiency during dry periods. The storage of water and capillary irrigation of these systems maintain high ratios of the latent heat flux during dry periods, which contribute to the cooling effect. In comparison, conventional green roofs were found to contribute more to an increase of the air temperature, due to a larger sensible heat flux than the blue-green roofs. It is found that the latent heat flux from the conventional green roof consumes only 46% of the net radiation energy during daytime, while the blue-green roof consumes almost 80%. The blue-green roof, with storage and capillary irrigation, is more efficient than the conventional green roof and changes the microclimate of the green roof significantly. We therefore conclude that water availability is crucial for green roofs to be an effective climate adaptation measure.

Master Thesis

Thijs van Veen

4021045

Under the supervision of:

Prof. dr. ir. Marc Bierkens from University Utrecht

Dr. ir. Gijsbert Cirkel from KWR Watercycle Research Institute

MSc. Bernard Voortman from KWR Watercycle Research Institute

24 February 2018

Table of Contents

1. Introduction

Global warming and on-going urbanization will result in an increase of the "Urban Heating Island" (UHI) effect (Kleerekoper et al, 2012; Santamouris, 2014). The UHI effect is known as the phenomenon that the urban temperature is higher than the surrounding rural environment, due to modification of land surfaces (i.e. application of energy absorbing surfaces such as asphalt and concrete on roofs and pavements, changes in reflection and absorption due to the geometry of build-up areas), generation of excess heat and lack of evapotranspiration. The extent of the temperature difference varies in time and space as a result of meteorological and surface characteristics of the urban area (Kleerekoper et al., 2012). An increase in the UHI effect results in a higher demand of electricity for cooling mechanisms, more air pollution and a higher ratio of mortality and/or illness because of heat stress (Hogrefe et al., 2004; Nowak et al., 2000; Rosenfeld et al., 1995; Rosenzweig et al., 2009; Sailor et al., 2002).

Another emerging problem in many cities is flooding. During heavy rainfall events, runoff exceeds the capacity of the sewer systems. This produces overflowing, nuisance and serious water pollution problems. The high stress on the sewer system is caused by the lack of permeable ground in the city limiting infiltration of rainwater (Scholz, 2004). According to van den Hurk et al. (2014), heavy rainfall events will occur more often in the future and air temperatures will rise. Therefore, we expect more stress on the sewer system and an increase of the UHI effect.

There are several options to decrease the UHI effect and decrease peak flows in sewer systems. One of these options is to reserve more space for permeable green areas in a city (Kleerekoper et al., 2012). Permeable ground decreases the peak discharge of rainfall events, because the amount of runoff reduction depends on the capacity for water interception, water retention and evapotranspiration (Chen et al, 2015; Nagase & Dunnett, 2012; Graceson et al., 2013).

Green roofs appear to be a promising solution, presenting a relatively high heat island mitigation potential (Costanzo et al., 2016; Santamouris, 2014). Research on green roofs has developed over the years: vegetation has been evaluated to reduce runoff from green roofs (Nagase & Dunnett, 2012), the cooling effect of cool roofs, "white/high albedo roofs", have been compared with green roofs (Santamouris, 2014), the energy aspects of a green roof for the benefit of the building itself are determined (Saadatian et al., 2013) and Li et al. (2014) proved that green roofs with relatively abundant soil moisture have comparable effect in reducing the surface and near-surface UHIs to cool roofs with an albedo value of 0.7. The services that are provided, including air pollution mitigation, storm-water management and reducing the UHI effect, are directly linked to evapotranspiration processes (Jim & Chen, 2008, 2009). Increasing the evapotranspiration and latent heat flux will cause a decrease of the sensible heat flux. However, rooftops are harsh environments for plants since the availability of water is limited and roofs are exposed to wind and solar radiation (Rowe, 2011; Vijayaraghavan, 2016).

Not all literature agrees on the efficiency of green roofs. Coutts et al. (2013) suggests to use cool roofs with good insulation instead of green roofs. The high albedo of a cool roof reduces the net radiation, leaving less energy available at the surface for sensible heating during the day, compared to green roofs. Solcerova et al. (2017) state that extensive sedum-covered green roofs might help decrease air temperatures at night, when the urban heat island is strongest, but possibly contribute to high daytime temperatures. However, Solcerova et al. (2017) also suggests that the availability of water in the substrate plays an important role in the cooling behaviour of the vegetation.

Increasing the evapotranspiration efficiency of a green roof could be the key for reducing the UHI effect. We hypothesise that an increase of the evapotranspiration efficiency can be found in the water availability of a green roof. Without the presence of water, evapotranspiration will not occur. For this reason, an extensive green roof is designed that consists of three different setups. Setup one and three are both equipped with a passive irrigating storage system (from permavoid), but differ in substrate thickness. Setup two is a

conventional green roof equipped with a simple drainage layer and a relatively thin substrate. Setup two is used as a comparison with the storage system. The actual evapotranspiration of the setups is determined using weighing lysimeters and the potential evapotranspiration is derived by parameterizing the Penman-Monteith (1965) equation with measured on-site climatic data. The objective of this thesis is to evaluate the efficiency of green roofs with a storage system to ensure optimal water availability compared to a conventional green roof. Furthermore, we want to provide valuable insight on the energy balance of a green roof with respect to a storage system and different substrate thicknesses.

2. Method and measurements

2.1General setup

The green roof is located in Amsterdam, the Netherlands (52.37° latitude, 4.92° longitude). The climate is known as a maritime climate with cool summers and moderate winters. The roof is six meters above sea level and has an area of 439m^2. Three different setups of 18.15 m^2 each were made on the green roof (see figure 1). Setup two is the conventional green roof, consisting of a four cm substrate with vegetation and a drainage layer. Setup one and three are equipped with a passive irrigating storage system from Permavoid. Setup one has a substrate thickness of eight cm and setup three of four cm. See Appendix A for the construction of the green roof.

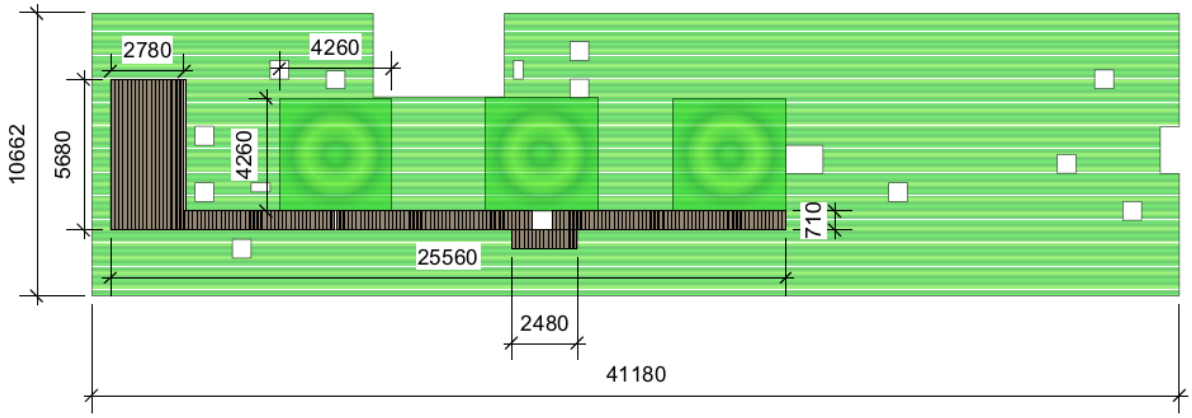

Figure 1. Schematic top view green roof. Setup one to three are the squares from left to right. The sizes are given in mm. Source: KWR Watercycle Research Institute.

To determine the efficiency of the evapotranspiration of the green roof, the actual evaporation, measured with the weighing lysimeters, is used as reference evapotranspiration of the green roof. With the onsite climatic measurements, the potential evapotranspiration is derived by parameterizing the Penman-Monteith equation.

The evapotranspiration is directly linked to the latent heat flux and the residual flux of the energy balance is assumed as the sensible heat flux. We present the latent heat flux (LE), the soil heat flux (G) and the sensible heat flux (H) as fractions of net radiation (Rn) based on linear regressions forced through zero. The microclimatic change of the green roof is determined using the "Bowen ratio".

Climatic data from "The Royal Netherlands Meteorological Institute" (KNMI) is used to extrapolate the behaviour of the green roof setups, reaching longer time periods than the onsite measurements. Data from the KNMI contains the potential evaporation from Makkink. The actual evaporation is derived from the Makkink evaporation using a simple bucket evaporation model. For validation, the climatic data of the KNMI is compared to the measured actual evaporation.

2.2 Permavoid system

"The permavoid capillary cell is a shallow, load-bearing, modular geocellular unit" (Atwood, 2017). The units have 92% of free space and are made to withstand an exceptional high compressive and tensile strength. This makes it possible to even build on it. Water stored inside the unit is afterwards used as passive irrigation for the vegetation, which is on top of the system.

The maximum storage of the permavoid unit is eight cm. A storage of three cm has been accomplished for this green roof. More storage would result in exceedance of roof weight regulations. Water that exceeds the maximum storage level is discharged to the sewer system.

The capillary cones are made of hydrophilic rockwool fibres. They are placed inside tubes within the permavoid units, which have an opening at the bottom and the top. Capillary force moves the stored water upwards through the capillary cones, until it reaches the geowicking textile.

The geowicking textile is a 3.6 mm thick textile that covers the permavoid units and prevents substrate from entering the permavoid units. It is a heavy-duty, non-woven, needle punched geotextile made from a blend of modified polyester fibres that are specifically formulated to absorb water and irrigate the mineral substrates that are on top of it (Atwood, 2017). The main purpose of the textile is to transport water laterally from the capillary cones. Note there is a maximum lateral distribution when plants take up water from the textile; water in the textile is replenished by the discharge of the capillary cones. However, when the demand of plants is higher than the capacity of the cones, the textile won't reach its maximum lateral distribution. To avoid this from happening, the amount of cones can be increased from two to four cones per unit, depending on vegetation demand.

The entire roof and the sides of the permavoid units are covered by a watertight sheet to make the blue-green roof watertight. Success of the permavoid units is dependent on the climatic conditions, where evaporation is required to empty the storage volume of the units and to prepare the roof to be able to store water for upcoming rain events.

2.3 Substrate and vegetation

Setup one and three have the same system but differ in substrate thickness. Setup one has a thickness of eight cm and setup three has a thickness of four cm. The conventional green roof has the same substrate thickness as setup three. The substrate used is produced by Optigrün gmbh and consists of shale, pumice, lava rock, crushed bricks, clay and compost. The substrate properties are known as a field capacity of ~21%, a porosity of ~64% and a density of 970 kgm^{-3} (Optigrün, 2013), following the German guidelines for green roof sites (FLL, 2008). The heat capacity of the substrate is assumed to be similar to "substrate 1" used by Sandoval et al. 2017: 931$MJm^{-3}K^{-1}$, which is given the density equal to 960 $Jkg^{-1}K^{-1}$.

All three of the set-ups have extensive vegetation of sedum, grasses and herbs. The initial vegetation present on the green roof consisted of sedum carpets delivered by Sempergreen. After placement of the sedum carpets, other native plants were sown on the sedum carpet/substrate to increase the biodiversity and give insight in the change in vegetation (plant competition) over time. For the complete list of plants, we refer to Appendix B. Sedums are commonly used plants on green roofs and most sedums are able to withstand long droughts because they are C3/"Crassulacean Acid Metabolism" (CAM) intermediate plants. Undergoing CAM induction when water is limited, but operating C3 photosynthetic pathways when water is abundant (Cushman & Borland, 2002).

2.4 On site measurements

In this thesis, the evapotranspiration is defined as the sum of soil evaporation, transpiration and canopy evaporation from interception. The direct measurement of evapotranspiration is achieved by on-going monitoring of a small scale weighing lysimeters, which are placed in the middle of the setups. The lysimeters have a surface area of 0.33 m^2. The green roof media is placed on top of the weighing lysimeter load cells to log the mass differences over time.

The 5TE sensor, from decagon devices, is used to measure the soil water content, the soil temperature and deriving the soil heat flux. The plate depth of the 5TE sensor is placed near the bottom of the substrates for all the setups. The soil moisture content is measured in values of permittivity. To retrieve the soil water content from the permittivity, the following equation yields (Kargas et al., 2013):

$$\theta = \frac{\sqrt{\varepsilon} - \alpha_0}{\alpha_1} \quad (1)$$

Where θ is the soil moisture content [-], ε the permittivity and the α values are soil dependent. The values for α_0 and α_1 are retrieved from substrate 2 used by Kargas et al. (2013), calculated with time domain frequency

models. The substrate from Kargas et al. (2013) is equal to the substrate present on the green roof and shows the same moisture contents as the known substrate properties (Optigrün, 2013). The values used for α_0 and α_1 are 1,64 and 10,97 and is based on a two-point calculation.

With the temperature measurements on the soil surface and underneath the soil, the heat storage (S) [Wm^2] is estimated. The sum of the soil heat flux beneath the soil and the storage (S) represent the soil heat flux (G) [Wm^2] at the surface.

A weather stations and additional sensors are positioned on the setups next to the lysimeters, measuring the air temperature, wind speed, wind direction, air moisture, air pressure, net radiation, incoming solar radiation and the infrared radiation. The air temperature is measured at three different heights; 21.5 cm**,** 54 cm and 150 cm. The wind speed, wind direction, air moisture and air pressure are measured at a height of 1.5 m. All the measurements are done with a five-minute interval, giving the average value over the measured time. Except for the rain, which gives the sum of a five-minute interval. The rain is measured with a tipping bucket.

Table 1. On-site measurements

Climatic conditions	**units**		**climatic condition**	**units**
precipitation	mm		Air pressure	mbar
Evapotranspiration	mm		Soil moisture	Fm^{-1}
Temperature (soil and air)	°C		Soil weight	g
Wind direction	°		Net radiation	Wm^{-2}
Wind speed	ms^{-1}		Incoming solar radiation	Wm^{-2}
Air moisture	%		Infrared radiation	Wm^{-2}

2.5 Penman-Monteith parameterization

The Penman-Monteith equation is used to model local potential evapotranspiration:

$$ET_p = \frac{\Delta(Rn-G)+\rho_a c_p(e_s-e_a)/r_a}{\left(\Delta+\gamma\left(1+\frac{r_s}{r_a}\right)\right)\lambda\rho_w} \quad (2)$$

Where ET_p is the potential evapotranspiration [mms^{-1}], Δ is the slope of saturation vapour pressure vs. temperature curve [$kPa°C^{-1}$], R_n is the net radiation [Jm^{-2}], G is the soil heat flux [Jm^{-2}], ρ_a is the air density [$kg\ m^{-3}$], c_p is the specific heat of moist air [$Jkg^{-1}°C^{-1}$], e_s is the saturation vapour pressure of the air [kPa], e_a is the actual vapour pressure of the air [kPa], r_a is the aerodynamic resistance to turbulent heat and vapour transfer [$s\ m^{-1}$], r_s is the surface resistance [sm^{-1}], γ is the psychrometric constant [$kPa°C^{-1}$], λ is the latent heat of vaporization [Jkg^{-1}] and ρ_w is the density of liquid water [kgm^{-3}].

Two different methods are applied to parameterize the Penman-Monteith equation. The first one relies on parameterizing the albedo, soil heat fraction and the surface resistance, which is referred to as the parameterized Penman-Monteith. The albedo is used to derive the net radiation. The value used for the albedo is set to 0.20 (Gaffin et al., 2009) and is representative for a sedum surface. The soil heat fraction is derived with a linear regression forced through zero, where the net radiation is placed on the x-axis and the soil heat flux on the y-axis. This is done for day and night time.

The second parameterisation relies on the on-site measurements from the green roof, which is referred to as the “measured” Penman-Monteith. For the measured Penman-Monteith, the climatic data is aggregated from a five-minute interval to an hourly.

Interception and through fall are calculated in mm, maximum interception is assumed to be 0.25 mm, which is equal to the interception of a dry grassland (Voortman et al., 2015). This maximum interception is used due to the lack of literature that is available for sedums.

2.5.1 Aerodynamic resistance

The transfer of heat and water vapour from the evaporating surface into the air above the canopy is determined by the aerodynamic resistance (Monteith & Unsworth, 1990):

$$r_a = \frac{\ln\left[\frac{z_m - d}{z_{om}}\right] \ln\left[\frac{z_h - d}{z_{oh}}\right]}{k^2 \, u_z} \tag{3}$$

Where r_a is the aerodynamic resistance [sm^{-1}], z_m is the height of wind measurements [m], z_h is the height of humidity measurements [m], d is the zero plane displacement height [m], z_{om} is the roughness length governing momentum transfer [m], z_{oh} is the roughness length governing transfer of heat and vapour [m], k is the von Karman's constant equal to 0.41 [-] and u_z is the wind speed at height z [ms^{-1}].

The height of the wind measurement equipment and the humidity measurements is 1.5 meter. The d, z_{om} and the z_{oh} are calculated with the FAO-56 approach (Allen et al., 1998):

$$d = \frac{2}{3} \, h \tag{4}$$

$$z_h = 0.123 \, h \tag{5}$$

$$z_{oh} = 0.1 \, z_{om} \tag{6}$$

Where h [m] is the height of the vegetation. The vegetation height used is 0.12 m.

2.5.2 Surface resistance

The surface resistance is the resistance of vapour flow through the transpiring crop and the evaporating surface (Allen et al., 1998). The r_s is back-calculated by isolating the r_s from the Penman-Monteith equation (2) given by:

$$r_s = \left(\left(\left(\frac{\Delta (R_n - G) + \rho_a c_p \left(\frac{e_s - e_a}{r_a} \right)}{ET * \lambda * p_w} \right) - \Delta \left(\frac{1}{\gamma} \right) \right) - 1 \right) * r_a \tag{7}$$

Where ET is the measured evaporation flux [$mmday^{-1}$]. Setup two is used to derive the surface resistance, because this setup had a constant vegetation cover of sedum. Determining the surface resistance of setup two gives a surface resistance for sedum.

The surface resistance calculated is a daily value and must be converted to daytime and night time values. The FAO uses a r_s of 50 [sm^{-1}] for day time and the value for daily estimates is 70 [sm^{-1}]. The night time value is considered representative for a moist and damp soil surface underneath a grass cover (ASCE, 2005). We assumed that the same value is representative for moist substrate underneath sedum. For calculating the surface resistance of the sedums during daytime, the same ratio between daytime and daily is used for the grassland. This yields a ratio of 50 divided by 70 (0.71). The unknown daytime value is than calculated as a cross table function:

$$r_s \, (day \; time) = \frac{50 * r_s(24H)}{70} = x \; \left[\frac{s}{m}\right]$$

The surface resistance is linked to the amount of water present. In case of water stress, the surface resistance increases. It is important to determine the surface resistance for days where potential evaporation applies. It is assumed, for this roof, that potential conditions apply to days following a rain event of five mm, interception evaporation had already been evaporated and water is not limiting. A rain event of five mm is expected to be sufficient to saturate the soil. When the soil is saturated, the actual evaporation is assumed to be in agreement with the potential evaporation for at least one day in summer.

2.6 Energy balance

The energy balance for the green roof is given by:

$$R_n = LE + H + G \tag{8}$$

Where R_n is the net radiation Wm^{-2}, LE is the latent heat flux in Wm^{-2}, H is the sensible heat flux in Wm^{-2} and G is the soil heat flux in Wm^{-2}. The sensible heat flux is given as a residual of the energy balance:

$$H = R_n - LE - G \quad (9)$$

Heat loss, as result of the warming of water inside the permavoid units and energy exchange due to metabolic activities, is neglected since the fraction will be near zero (Hillel, 1980; Ayata et al., 2011). The energy balance is used as an 1D flux system for simplicity, where radiation goes in and out. In reality, the balance is in 3D due to the fact that air is always in movement. This Influences the sensible heat flux and the latent heat flux. However, this is very difficult to simulate and stretches beyond the aims of this study.

The energy balance is derived for daytime conditions, because it is assumed that the latent heat flux happens during daytime. Hourly data was aggregated to day- and night time values, which are based on the net radiation. Periods with a positive net radiation are considered as daytime and periods with a negative net radiation are considered as night time. It is assumed that the latent heat flux is negligible during night time. This means that latent heat flux (evapotranspiration) is only during daytime.

2.7 Bowen ratio

Neglecting the soil heat flux, which is near zero when averaged over a day (Campbell, 1977), net radiation can be partitioned between sensible and latent heat. This partitioning of energy is commonly expressed as the Bowen ratio (see equation 10) and yields valuable information on the microclimate prevailing at the Earth's surface (Bristow and Campbell, 1983). The Bowen ratio is the ratio of sensible heat divided by latent heat (Tanner et al. 1987; Kustas et al., 1996; Perez et al, 1999):

$$\beta = \frac{H}{LE} \quad (10)$$

Where β is the Bowen ratio [-], H is the sensible heat in Wm^{-2} and LE is the latent heat in Wm^{-2}. The result of the Bowen ratio defines what class of environment is dealt with. When the ratio becomes smaller than one, the environment is known as humid. When the Bowen ratio becomes greater than one, the environment becomes drier.

2.8 Extrapolating data

To ensure the quality of measurements on a longer time scale, extrapolated data is compared to the weighing lysimeter evapotranspiration and the potential evapotranspiration. The climatic data used is derived from the KNMI, and consists of net precipitation and the potential evaporation (Makkink). The collected data originates from a meteorological station at Schiphol Airport, which is located 15 kilometres South-East from the green roof.

The actual evaporation is determined with a simple bucket model based on Ireson & Butler (2013). It consists of a balance equation with evaporation and drainage as outgoing flux and precipitation as incoming flux. The Root Constant (RC) is the minimum volume of water needed for plants to potentially evaporate and is assumed to be reached when 10 mm of water remains in the bucket. The actual evaporation of the model reduces linearily when the RC is reached, otherwise the actual evaporation is the same as the potential evaporation. The permanent wilting point (PWP) is the maximum volume of the bucket, which depends on the volume of the setup. When the permanent wilting point is reached, the evapotranspiration stops.

The bucket and the Makkink evaporation were compared with the measured actual evaporation from the weighing lysimeter for validation. Afterwards, the Makkink evaporation is also compared with the parameterized Penman-Monteith and the measured Penman-Monteith to look for similarities.

The period that is used for calculating the average climatic conditions is from 1990 to 2017. Determining the potential evaporation (Makkink), actual evaporation (bucket) and the precipitation gives insight in the efficiency of the green roof. The maximum storage (eight cm) is also added to the average climatic conditions. By adding the maximum storage to the average climatic conditions, a comparison can be made between the different storages that gives insight in the water efficiency.

3. Results

3.1 Actual evaporation vs. measured Penman-Monteith

The on-site 'measured' potential evapotranspiration and the measured evapotranspiration from the lysimeter for all three set-ups are given in figure 2. The surface resistance retrieved from selected periods in June, July and August, is 170 [s/m]. Adding this value for the r_s(24H) in equation 7 results in a r_s (day time) of 120 [sm^{-1}], which is used for calculating the measured Penman-Monteith. Accuracy difficulties were encountered with the soil moisture content (see appendix C). Which could lead to a 10% increase in soil heat flux. Note that this has low impact since it is the result from the net radiation minus the soil heat flux and soil heat flux is only changing 0.6% – 0.85% (see table 2 "day time").

For the first two months, the actual evaporation from setup one and three agree well with the measured potential evaporation. After two months, the measured evapotranspiration becomes greater than the potential evaporation. However, setup three shows one moment, a few days before September, where the actual evaporation becomes smaller than the potential evaporation.

The actual evaporation and the measured potential evaporation of setup two agree most of the time. However, the measured potential evaporation keeps high rates, while the actual evaporation reduces. This is shown in the first two months for an extended period during a dry spell.

The gaps in between the measured evapotranspiration lines are inaccurate measurements, external problems and rain events resulting in no data points. Heavy rain events cause drainage of the substrate. The substrate is not able to maintain the water, since the field capacity is exceeded. The water drains into the permavoid. However, when the maximum storage is exceeded, the water flows out of the system. This process results in inconsistent data until the drainage stops.

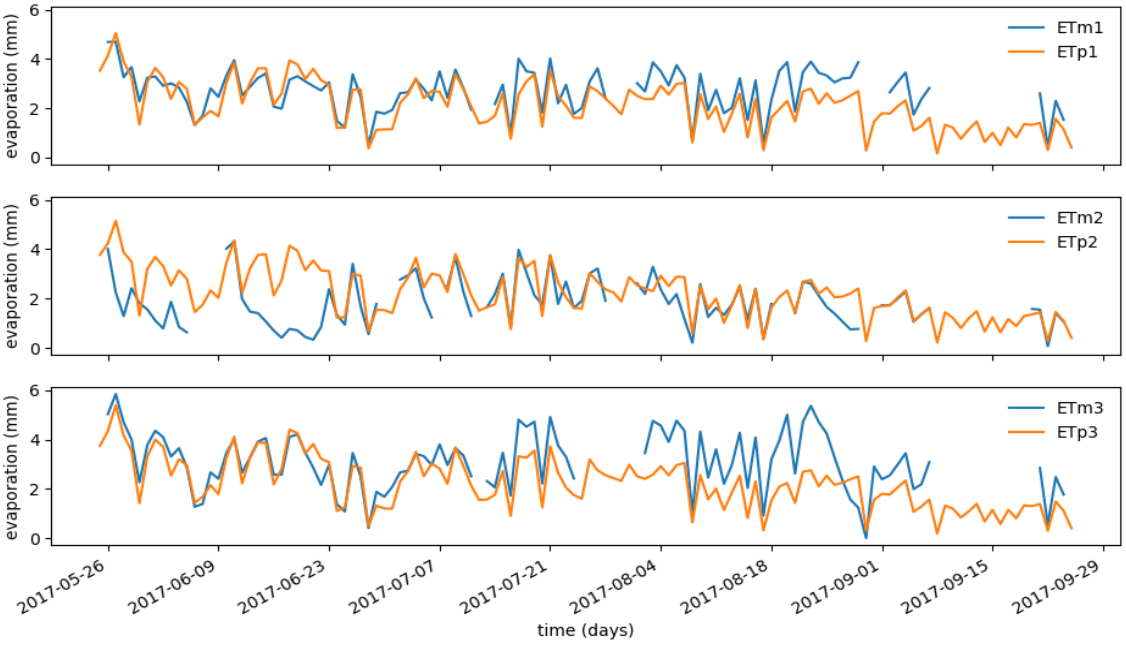

Figure 2. Lysimeter evaporation (ETm) vs. measured Penman-Monteith evaporation (ETp), with setup one on top and setup two and three beneath.

3.2 Energy balance

Figure 3 shows the energy balances of the setups during daytime. The latent and the sensible heat flux have a different pattern on all the setups, but a clear relation is visible. When the latent heat flux is great, the sensible heat flux is small, exhibiting an inverse relationship. For both setups (one and three) the latent heat flux is

greater than the sensible heat flux in the first two months. Afterwards, during August and September the latent heat flux can even become greater than the net radiation, resulting in negative values for the sensible heat flux.

Setup two has greater sensible heat fluxes than latent heat fluxes in the end of May and June. The latent heat fluxes are slightly higher than the sensible heat fluxes during July, August and September. The soil heat fluxes are similar for all the setups.

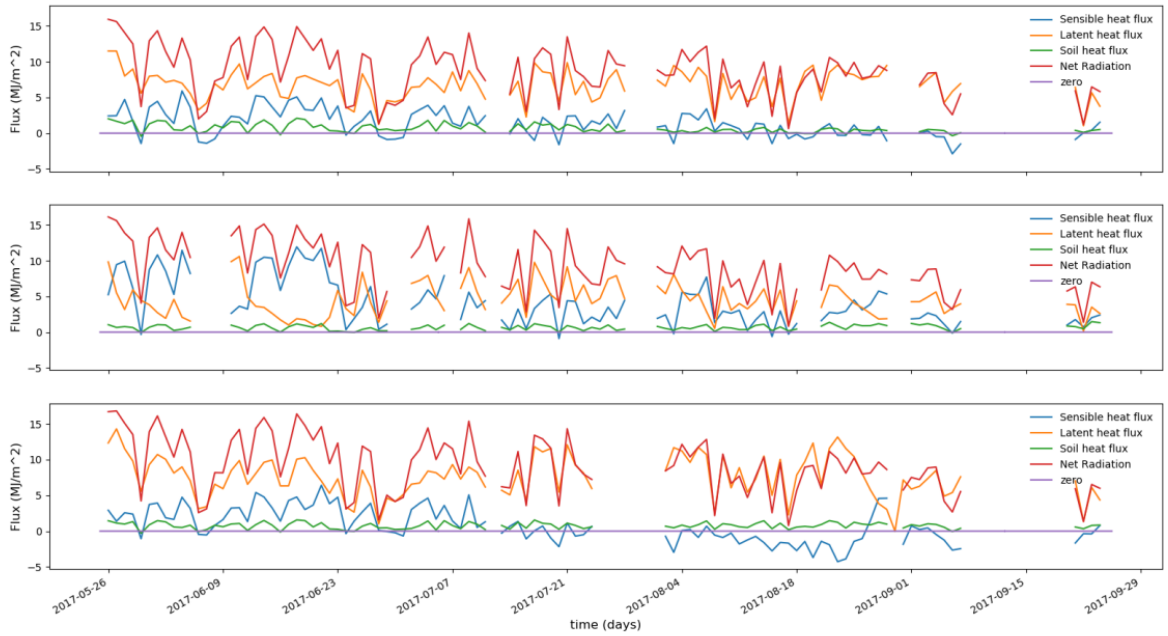

Figure 3. Energy balance of the setups during daytime.

3.2.1 Day and night fractions

The net radiation that enters the green roof is in balance with the latent heat flux, the sensible heat flux and the soil heat flux. The fractions are given in table 2, which are divided in day time, night time and daily. Appendix D shows the linear regression analyses for setup one during day time, Appendix E is with respect to setup two and Appendix F shows the results of setup three.

Day time

The fraction of energy that is consumed by the soil heat flux is small. A slight difference of the fractions is noticed between the setups. Setup two has the lowest fraction and setup one is 0.023 higher than setup three.

The fraction of energy that goes into the latent heat flux is greater for setup one and three than for setup two. The difference between setup one and three is also significant. The fraction of energy that is used for sensible heat is the opposite order than the latent heat flux. Note that the fraction of the latent heat flux and the sensible heat flux are almost even for setup two.

Night time

The night time fractions are derived from the negative net radiation. The sensible heat flux is greatest for setup one and smallest for setup three. For the ground heat flux, the opposite is demonstrated.

Daily (24 hours)

On a daily basis, a very small fraction is used for the soil heat fraction. It is constant and applies to all the setups. However, the latent heat flux and the sensible heat flux show great differences when comparing the setups. Setup three has the greatest latent heat flux; 91.99% of the net radiation is used for evapotranspiration and only 6.51% went into the sensible heat flux. Setup one has a sensible heat flux that is double the fraction of setup three and setup two has a sensible heat flux that comes close to the latent heat flux.

The reason that setup one and setup three have such great latent heat fluxes is due to the change between day and night. Daily values are averaged over day and night. The values during day time are positive, while the

night time values are negative. When day time and night time are averaged out, they will be close to zero. The latent heat flux is not averaged out with negative values, because the latent heat flux is assumed to occur during day time and is zero during night time. This results in high positive values for the latent heat flux and high fractions from the net radiation. This might lead to an overestimation towards the latent heat flux.

Table 2 Flux fractions of the net radiation.

		Fraction of net radiation					
Setup	Flux	Day time		Night time		Daily	
1	G	0.0842	8.42%	0.2817	28.17%	0.0096	0.96%
	LE	0.7237	72.37%	0%	0%	0.854	85.40%
	H	0.1921	19.21%	0.7183	71.83%	0.1364	13.64%
2	G	0.0685	6.85%	0.3307	33.07%	0.0142	1.42%
	LE	0.4614	46.14%	0%	0%	0.5397	53.97%
	H	0.4701	47.01%	0.6693	66.93%	0.4461	44.61%
3	G	0.0819	8.19%	0.368	36.80%	0.015	1.50%
	LE	0.7879	78.79%	0%	0%	0.9199	91.99%
	H	0.1302	13.02%	0.632	63.20%	0.0651	6.51%

3.2.3 Bowen ratio

The results of the Bowen ratio are given in figure 4 and are relevant for day time, since the latent heat flux is assumed to be zero during night. Setup one and three show a similar pattern and, most of the time, stay in between zero and one. Many slightly negative values are observed during August, in particularly for setup three and to a lesser extend setup one. Setup three shows one period with a Bowen ratio above one, while setup one stays near zero. In contrary to setup up one and three, setup two is recognized with higher Bowen ratios that increase per day. Setup two even shows short periods with extremely high Bowen ratios.

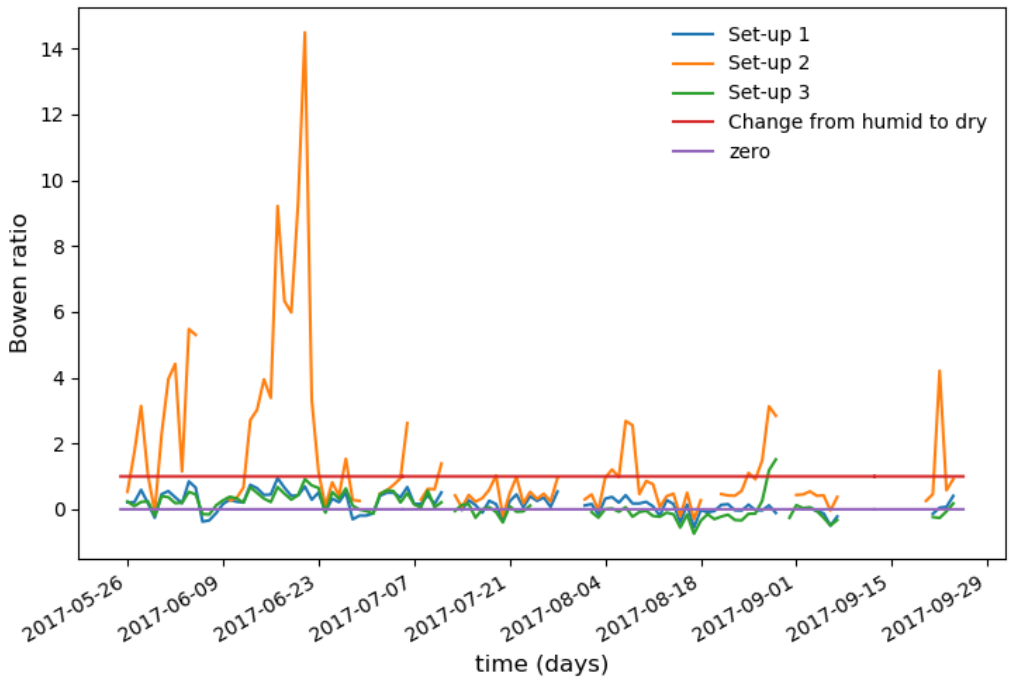

Figure 4. Bowen ratio (H/LE).

3.3 Extrapolating data

Figure 5 shows the measured evaporation (lysimeter), the bucket evaporation and the Makkink evaporation. The similarities of the measured and the bucket evaporation are remarkable in this setting. The Makkink evaporation is greater than the measured evaporation for the first two months. Afterwards, the measured evaporation of setup one and three becomes greater than the Makkink evaporation, while the measured evaporation of setup two agrees with the Makkink evaporation.

In figure 6, the potential evaporation methods are compared. The parameters of the parameterized Penman-Monteith are placed in table 3. The Makkink evaporation shows the highest values most of the time. The Parameterized Penman-Monteith is almost equal to the Makkink evaporation, while the measured Penman-Monteith shows lower values.

Table 3. Left: Parameters from the parameterized Penman-Monteith.
Right: Permanent wilting point (PWP) and root constant (RC) data per setup.

Parameter	value
Albedo	0.20
Soil heat fraction day	0.0685
Soil heat fraction night	0.3307
Surface resistance day	120 sm^{-1}
Surface resistance night	200 sm^{-1}

Setup	PWP	RC
1	60	70
2	10	20
3	40	50
1 max	110	120
3 max	90	100

The average weather conditions, concerning Makkink evaporation, bucket evaporation and precipitation, are shown in figure 7. The used climatic data is from 1990 to 2017, due to the fact that the Makkink evaporation measurements had started at Schiphol in 1990. Otherwise, an average of 30 years would have been considered. The results for the RC and the PWP are given in table 3, which are derived from the lysimeter measurements. The potential evaporation of Makkink is greater than the actual evaporation from the bucket model. The greater the storage, the less evaporation deficit.

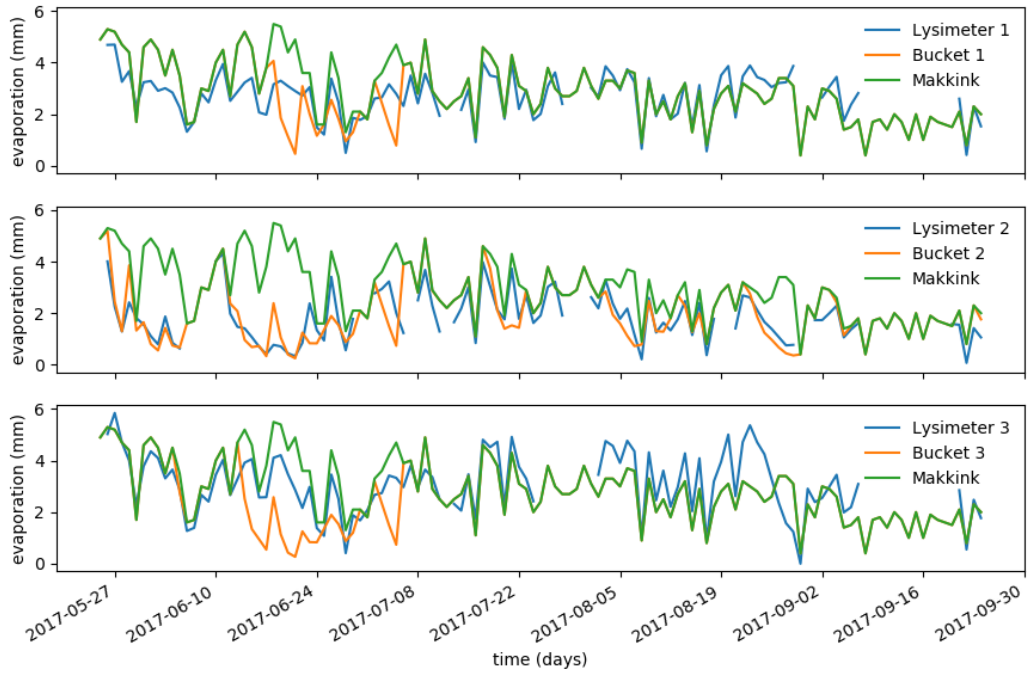

Figure 5. Makkink evaporation vs. actual bucket evaporation and actual lysimeter evaporation from setup one to three.

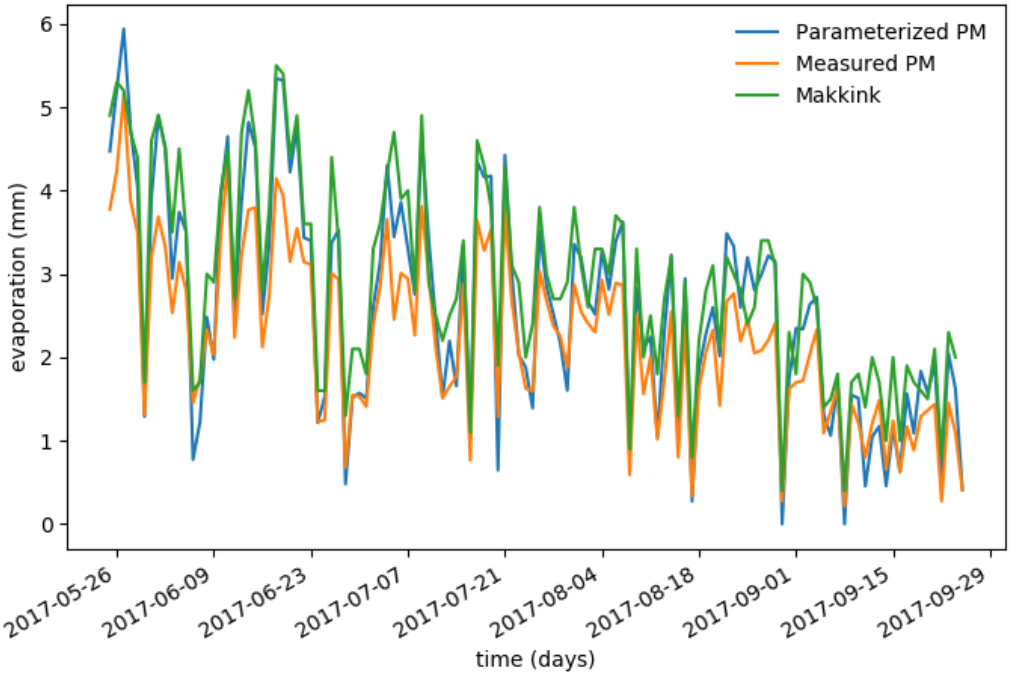

Figure 6. Makkink evaporation vs. potential evaporation of parameterized Penman-Monteith and measured Penman-Monteith on setup two.

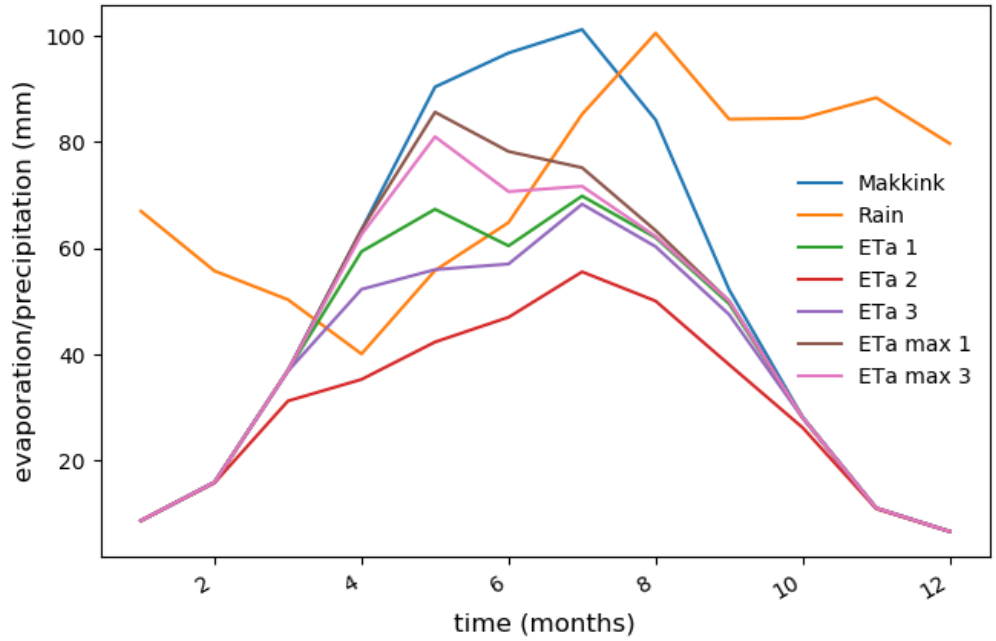

Figure 7. Average meteodata 1990-2017, with Makkink as the potential evaporation and ETa for the actual evaporation of that setup. ETa max yields for the maximum storage of eight cm.

4. Discussion

4.1 Actual evaporation vs. measured Penman-Monteith

The potential evapotranspiration is sometimes greater than the actual evapotranspiration. These events can be explained with water limitations of the soil. During dry periods when evapotranspiration occurs, the soil moisture content decreases rapidly. If the wilting point is reached, caused by less water in the soil, vegetation

stops transpiring and the remnants of water evaporates by soil evaporation until the soil is dry. This process causes the reducing line of the actual evapotranspiration (see figure 2), which we refer to as a dry out event.

The many dry out events for setup two are caused by the lack of water storage. When water is available during drought, vegetation starts evapotranspirating quickly until water becomes limited. Water shortage causes a decrease of the evapotranspiration rates. This is shown in setup two with a reduction of the actual evaporation, while the potential evaporation remains high.

Setup three still has one dry out event, even when equipped with a storage system. A dry out event occurs in setup one and three when there is more evaporation than precipitation for an extended period. The limited amount of precipitation then causes an evaporation deficit/dry out event. However, the evaporation deficit must be greater than the amount of water that is stored for causing a dry out event. Setup one contains no dry out events, because the substrate layer of setup one is twice as thick as the one at setup three. This difference in substrate thickness allows setup one to store 20 mm more water than setup three.

Besides the difference in storage, setup one and three also differ in the amount of evapotranspiration. Setup three has higher evapotranspiration rates than setup one. The difference in evapotranspiration can be explained by a mulching effect of the soil. The 4 cm substrate has, by definition, a higher water content at the surface than the 8 cm substrate. The higher the soil moisture near the surface, the more water will be evaporated. The mulching effect is more pronounced at setup one. Due to the substrate thickness, the top of the substrate is able to dry out which limits soil evaporation.

After July, setup one and three show higher actual evaporation rates than potential evaporation, which can be explained by a changing surface resistance. The surface resistance used for the measured Penman-Monteith is based on a sedum vegetated surface. However, the vegetation of plot one and three changed over time due to germination of (C3) grasses and herbs, while setup two stayed sedum dominated due to water stress. The change of vegetation also changed the surface resistance**.** This might lead to an underestimation of the potential evaporation. Changing surface resistance with time would result in a better estimate of potential evapotranspiration for setup one and three.

4.2 Energy efficiency

The latent heat flux is dominant if water is abundant. This can be derived from figure 2 and figure 3 by comparing setup two with setup one and three. Within periods of drought, stored water is used to provide water to the plants and the soil at setup one and three, maintaining a high evapotranspiration and thus a high latent heat flux. Setup two shows a reduced latent heat flux during the same periods. During longer periods of drought, the setups with storage show a similar pattern; a reducing latent heat flux and an increasing sensible heat flux when the stored water becomes limited (see figure 3 at the end of August).

The energy efficiency of the green roof is illustrated using the Bowen ratio, which reveals the microclimatic conditions. When calculating the Bowen ratio, the soil heat flux is neglected due to the fact that it is the most constant flux (Campbell, 1977). This leaves the relation between the sensible heat flux and the latent heat flux. Small Bowen ratios, which can even be negative, are preferred since they are the result of greater latent heat fluxes. The negative values for the Bowen ratio (see figure 4) are explained by the “oasis effect” phenomena. An oasis effect occurs when evapotranspiration takes place on such a scale that external energy is used to increase the latent heat flux. The external energy source used in this case is sensible heat. The oasis effect is described as follows: “Warmth of the air is taken to increase the latent heat flux. When energy is taken from the air, air cools down. The cooling of air results in a negative sensible heat flux and it creates a cooler area than the surrounding”. This generates the opposite effect of the UHI, an Urban Cooling Island (Rosenfeld et al., 1995). The sensible heat flux is positive when the air absorbs energy, which increases the temperature of the air. This is in agreement with Wong et al. (2003), who found that the cooling effect of plants was confirmed by ambient air temperatures measured at different heights.

High Bowen ratios are directly linked to water limitations of the soil, since high sensible heat fluxes are dominant over the latent heat fluxes when there is less water available. Small Bowen ratios are linked to water abundance, because the latent heat flux is dominant over the sensible heat flux. Comparing the setups with this knowledge, it is clear that setup two, the conventional green roof, is not as efficient as setup one and three. Setup two is recognized with many dry out events and extremely high Bowen ratios, while setup one and three are recognized by low Bowen ratios that even become negative. Setup one and three contribute to cooling during dry periods, contrary to setup two, which contributes to an increase of the air temperature.

4.3 Extrapolating data

The Makkink evapotranspiration is greater than the measured Penman-Monteith and the parameterized Penman-Monteith, due to the fact that the Makkink evapotranspiration applies to a wet grassland and the measured- and parameterized Penman-Monteith apply for a sedum surface. However, the differences between the Makkink and the parameterized Penman-Monteith are small, while the measured Penman-Monteith is much lower. This can be explained by the accuracy of the parameters that are used for the measured- and the parameterized Penman-Monteith. The measured Penman-Monteith uses on-site measurements, which consider the conditions from that moment. This might result in a more accurate potential evaporation than the parameterized Penman-Monteith, which uses fixed values. With fixed values, the climatic conditions are considered less than with on-site measurements, which can result in an overestimation of the potential evapotranspiration.

The actual evapotranspiration derived with a simple bucket model agrees well with the actual evapotranspiration from the weighing lysimeter of setup 2. The bucket model shows a reduction period of the evapotranspiration in June for setup one and three, while the lysimeters measured evapotranspiration. The difference between the lysimeter and the Bucket model can be explained by the saturation of the storage. The vegetation on the green roof was watered after the dry period in May, because the sedum carpets had just been placed. Watering was needed to prevent the vegetation from drying out and give the vegetation a good start. However, the bucket model is derived over the whole year. During the dry period in May a large part of the storage is already evaporated from the bucket model. This resulted in an evapotranspiration deficit in June for the bucket model, while the green roof still had water stored due to the irrigation in May.

The average data from the past 27 years validate that even the storage system will face periods of water shortage or at least reduction of evapotranspiration. All the setups show an evapotranspiration deficit, even when the maximum storage of 80 mm is used. However, the data presented in figure 7 is the average evapotranspiration from 1990-2017. The average data contains biased data, due to the fact that very dry years result in a high evaporation deficit. These years put more weight towards an evaporation deficit, which might lead to an overestimation. For the precipitation, it is the other way around, where the wet years might cause an overestimation.

It is known that 40% of the precipitation falls during the first half of the year. During this period, there is more evaporation expected than precipitation, which can result in an evaporation deficit. A solution for increasing the evaporations rates to reach the potential evaporation can be found in overflow of water. The high amount of precipitation during the second half of the year can result in an overflow. This happens when the maximum storage is being exceeded. A system for reusing exceeded water will decrease or might even mitigate the evaporation deficit.

For better understanding of the processes that occur inside the green roof equipped with a storage system, it was intended to make a Hydrus model. However, the properties of the geowicking textile and the capillary cones are still unknown. For this reason, the Hydrus data is not used for the thesis, but given as extra results in Appendix G.

5. Conclusion

The objective of this thesis was to evaluate the efficiency of a green roof with a storage system to ensure optimal water availability compared to a conventional green roof. It is observed that the cooling efficiency of a green roof improves with a storage system. The cooling effect of a green roof is directly linked to the water availability. With an abundance of water, the storage systems can have a greater evapotranspiration then the potential evapotranspiration. The storage system maintains high evaporation rates during drought, whereas the conventional system shows a reduction of the evaporation. The substrate thickness has an important role in the evaporation rate as well. The thinner substrate of setup three has higher evaporation rates than setup one. However, the storage system is still reliable on precipitation. It is only able to withstand long periods of drought if there is enough water in the storage available. Otherwise the evaporation rates will reduce.

To reduce the UHI effect a dominant latent heat flux is desired, which is coupled to the evaporation. Whereas the sensible heat flux contributes to increasing heat, contributes the latent heat flux to remain/cool the air temperature. With the storage system high latent heat fluxes and low sensible heat fluxes are maintained, while the conventional green roof has a greater sensible heat flux. This means that the usage of a storage system improves the efficiency of a green roof significantly.

References

ASCE Task Committee on Standardization of Reference Evapotranspiration of the Environmental, Water Resources Institute. (2005). The ASCE standardized reference evapotranspiration equation, ASCE, Reston, VA.

Allen, R. G., Pereira, L. S., Raes, D., Smith, M., & Ab, W. (1998). Allen_FAO1998, 1–15. https://doi.org/10.1016/j.eja.2010.12.001

Atwood, J. (2017). Welcome to, (1996), 1–14. https://doi.org/10.1080/03632415.2015.1027159

Ayata, T., Tabares-Velasco, P. C., & Srebric, J. (2011). An investigation of sensible heat fluxes at a green roof in a laboratory setup. *Building and Environment*, *46*(9), 1851–1861. https://doi.org/10.1016/j.buildenv.2011.03.006

Bristow, K. L. and Campbell, G. S. (1983). On the relationship between incoming solar radiation and daily maximum and minimum temperature, *31*(427), 159–166.

Campbell, G.S., 1977. An Introduction to Environmental Biophysics. Springer-Verlag, New York.

Chen, X., Huang, P., Zhou, Z., & Gao, C. (2015). A review of green roof performance towards management of roof runoff. *Ying Yong Sheng Tai Xue Bao = The Journal of Applied Ecology / Zhongguo Sheng Tai Xue Xue Hui, Zhongguo Ke Xue Yuan Shenyang Ying Yong Sheng Tai Yan Jiu Suo Zhu Ban*, *26*(8), 2581–2590. Retrieved from https://www.scopus.com/inward/record.uri?eid=2-s2.0-84961006519&partnerID=40&md5=799925e65086b667a3352fcba49a097a

Costanzo, V., Evola, G., & Marletta, L. (2016). Energy savings in buildings or UHI mitigation? Comparison between green roofs and cool roofs. *Energy and Buildings*, *114*, 247–255. https://doi.org/10.1016/j.enbuild.2015.04.053

Coutts, A. M., Daly, E., Beringer, J., & Tapper, N. J. (2013). Assessing practical measures to reduce urban heat: Green and cool roofs. *Building and Environment*, *70*, 266–276. https://doi.org/10.1016/j.buildenv.2013.08.021

Cushman, J. C., & Borland, A. M. (2002). Induction of Crassulacean acid metabolism by water limitation. *Plant, Cell and Environment*, *25*(2), 295–310. https://doi.org/10.1046/j.0016-8025.2001.00760.x

FLL - Forschungsgesellschaft Landschaftsentwicklung Landschaftsbau. (2008). The new Guideline for The Planning and Upkeep of Green-Roof Sites (Overview). In *Federation of Green-Roof Associations, EFB, Conference Budapest 2008* (pp. 2–13).

Gaffin, S. R., Khanbilvardi, R., & Rosenzweig, C. (2009). Development of a Green Roof Environmental Monitoring and Meteorological Network in New York City. *Sensors*, *9*(4), 2647–2660. https://doi.org/10.3390/s90402647

Graceson, A., Hare, M., Monaghan, J., & Hall, N. (2013). The water retention capabilities of growing media for green roofs. *Ecological Engineering*, *61*(PA), 328–334. https://doi.org/10.1016/j.ecoleng.2013.09.030

HILLEL, D. (1980). *Applications of Soil Physics*. *Applications of Soil Physics*. https://doi.org/10.1016/B978-0-12-348580-9.50005-5

Hogrefe, C., Biswas, J., Lynn, B., Civerolo, K., Ku, J. Y., Rosenthal, J., … Kinney, P. L. (2004). Simulating regional-scale ozone climatology over the eastern United States: Model evaluation results. *Atmospheric Environment*, *38*(17), 2627–2638. https://doi.org/10.1016/j.atmosenv.2004.02.033

Ireson, A. M., & Butler, A. P. (2013). A critical assessment of simple recharge models: Application to the UK Chalk. *Hydrology and Earth System Sciences*, *17*(6), 2083–2096. https://doi.org/10.5194/hess-17-2083-2013

Jim, C. Y., & Chen, W. Y. (2008). Assessing the ecosystem service of air pollutant removal by urban trees in Guangzhou (China). *Journal of Environmental Management*, *88*(4), 665–676. https://doi.org/10.1016/j.jenvman.2007.03.035

Jim, C. Y., & Chen, W. Y. (2009). Ecosystem services and valuation of urban forests in China. *Cities*, *26*(4), 187–194. https://doi.org/10.1016/j.cities.2009.03.003

Kargas, G., Ntoulas, N., & Nektarios, P. A. (2013). Moisture content measurements of green roof substrates using two dielectric sensors. *HortTechnology*, *23*(2), 177–186.

Kleerekoper, L., Van Esch, M., & Salcedo, T. B. (2012). How to make a city climate-proof, addressing the urban heat island effect. *Resources, Conservation and Recycling*, *64*, 30–38. https://doi.org/10.1016/j.resconrec.2011.06.004

Kustas, W. P., Stannard, D. I., & Allwine, K. J. (1996). Variability in surface energy flux partitioning during Washita '92: Resulting effects on Penman-Monteith and Priestley-Taylor parameters. *Agricultural and Forest Meteorology*, *82*(1–4), 171–193. https://doi.org/10.1016/0168-1923(96)02334-9

Li, D., Bou-Zeid, E., & Oppenheimer, M. (2014). The effectiveness of cool and green roofs as urban heat island mitigation strategies. *Environmental Research Letters*, *9*(5). https://doi.org/10.1088/1748-9326/9/5/055002

Monteith, J. L. (1965). Evaporation and environment. *Symposia of the Society for Experimental Biology*, *19*, 205–234. https://doi.org/10.1613/jair.301

Monteith, J. L., & Unsworth, M. H. (1990). Principles of environmental physics, 2nd Edition. In *Edward Arnold, London* (p. 197). https://doi.org/10.1016/B978-0-12-386910-4.00026-3

Nagase, A., & Dunnett, N. (2012). Amount of water runoff from different vegetation types on extensive green roofs: Effects of plant species, diversity and plant structure. *Landscape and Urban Planning*, *104*(3–4), 356–363. https://doi.org/10.1016/j.landurbplan.2011.11.001

Nowak, D. J., Civerolo, K. L., Trivikrama Rao, S., Gopal Sistla, Luley, C. J., & E. Crane, D. (2000). A modeling study of the impact of urban trees on ozone. *Atmospheric Environment*, *34*(10), 1601–1613. https://doi.org/10.1016/S1352-2310(99)00394-5

Optigrün. (2013). Properties of the M-L Substrate.

Perez, P. J., Castellvi, F., Ibañez, M., & Rosell, J. I. (1999). Assessment of reliability of Bowen ratio method for partitioning fluxes. *Agricultural and Forest Meteorology*, *97*(3), 141–150. https://doi.org/10.1016/S0168-1923(99)00080-5

Rosenfeld, A. H., Akbari, H., Bretz, S., Fishman, B. L., Kurn, D. M., Sailor, D., & Taha, H. (1995). Mitigation of urban heat islands: materials, utility programs, updates. *Energy and Buildings*, *22*(3), 255–265. https://doi.org/10.1016/0378-7788(95)00927-P

Rosenzweig, C., Solecki, W. D., Parshall, L., Lynn, B., Cox, J., Goldberg, R., … Watson, M. (2009). Mitigating new york city's heat island integrating stakeholder perspectives and scientific evaluation. *Bulletin of the American Meteorological Society*, *90*(9), 1297–1312. https://doi.org/10.1175/2009BAMS2308.1

Rowe, D. B. (2011). Green roofs as a means of pollution abatement. *Environmental Pollution*, *159*(8–9), 2100–2110. https://doi.org/10.1016/j.envpol.2010.10.029

Saadatian, O., Sopian, K., Salleh, E., Lim, C. H., Riffat, S., Saadatian, E., … Sulaiman, M. Y. (2013). A review of energy aspects of green roofs. *Renewable and Sustainable Energy Reviews*, *23*, 155–168. https://doi.org/10.1016/j.rser.2013.02.022

Sailor, D. J., Kalkstein, L. S., Sailor, D. J., & Wong, E. (2002). The potential of urban heat island mitigation to alleviate heat related mortality: methodological overview and preliminary modeling results for Philadelphia. *Proceedings of the 4th Symposium on the Urban Environment*, (vol. 4), 68–69.

Sandoval, V., Bonilla, C. A., Gironás, J., Vera, S., Victorero, F., Bustamante, W., … Suárez, F. (2017). Porous Media Characterization to Simulate Water and Heat Transport through Green Roof Substrates. *Vadose Zone Journal*, *16*(4), 0. https://doi.org/10.2136/vzj2016.10.0101

Santamouris, M. (2014). Cooling the cities - A review of reflective and green roof mitigation technologies to fight heat island and improve comfort in urban environments. *Solar Energy*, *103*, 682–703. https://doi.org/10.1016/j.solener.2012.07.003

Scholz, M. (2004). Case study: Design, operation, maintenance and water quality management of sustainable storm water ponds for roof runoff. *Bioresource Technology*, *95*(3), 269–279. https://doi.org/10.1016/j.biortech.2003.07.015

Solcerova, A., van de Ven, F., Wang, M., Rijsdijk, M., & van de Giesen, N. (2017). Do green roofs cool the air? *Building and Environment*, *111*, 249–255. https://doi.org/10.1016/j.buildenv.2016.10.021

Tanner, B.D., Greene, J.P., Bingham, G.E., (1987) A Bowen ratio design for long term measurements Am. Soc. Agric. Eng. Tech. Paper No. 87-2503, ASAE, St. Joseph, MI

Vijayaraghavan, K. (2016). Green roofs: A critical review on the role of components, benefits, limitations and trends. *Renewable and Sustainable Energy Reviews*, *57*, 740–752. https://doi.org/10.1016/j.rser.2015.12.119

Voortman, B. R., Bartholomeus, R. P., Van Der Zee, S. E. A. T. M., Bierkens, M. F. P., & Witte, J. P. M. (2015). Quantifying energy and water fluxes in dry dune ecosystems of the Netherlands. *Hydrology and Earth System Sciences*, *19*(9), 3787–3805. https://doi.org/10.5194/hess-19-3787-2015

Wong, N. H., Chen, Y., Ong, C. L., & Sia, A. (2003). Investigation of thermal benefits of rooftop garden in the tropical environment. *Building and Environment*, *38*(2), 261–270. https://doi.org/10.1016/S0360-1323(02)00066-5

Appendix A: Construction of the green roof (source: KWR Watercycle Research Institute).

Figure A1 Bitumen roof, before construction of the green roof.

Figure A2 Placement of the permavoid units during construction of the green roof.

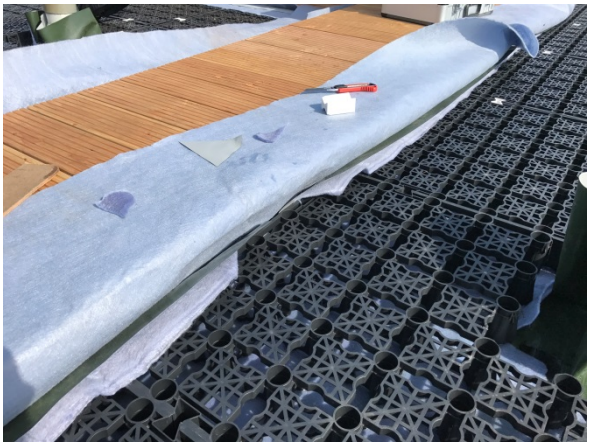

Figure A3 Placement of the geowicking textiles above the permavoid units.

Figure A3 Placement of the substrate and the setups. The square in the middle is the lysimeter with climatic measurements next to it.

Figure A5 After construction of the green roof

Appendix B: Vegetation green roof

Table B.1 Vegetation that is sown/grows on the green roof.

Mixture 1	**Mixture 2**	
Latin name	**Dutch name**	**Latin name**
achillea millefolium	Bieslook	allium schoenoprasum
allium schoenoprasum	steenanjer	dianthus deltoides
anthoxanthum odoratum	schapengras	Festuca ovina subsp. ovina
armeria maritima	fakkelgras	koeleria glauca
campanula rotundifolia	kalkdoddegras	Phleum boehmeri
Satureja vulgaris	blaasilene	silene vulgaris
dianthus armeria	reukgras	anthoxanthum odoratum
dianthus carthusianorum	reigersbek	erodium cicutarium
dianthus deltoides	robertskruid	Geranium robertianum
erigeron acer	vlas	Linum usitatissimum
erodium cicutarium	viltganzerik	Potentilla argentea
Festuca ovina subsp. ovina	muurpeper	sedum rupestre
Festuca rubra subsp. arenaria	grote tijm	thymus pulegioides
galium verum	zwenkdravik	Bromus tectorum
hieracium pilosella	hardzwenkgras	Festuca ovina subsp. cinerea
jasione montana	strobloem	Helichrysum arenarium
linaria vulgaris	wimperparelgras	Melica ciliata
Lotus corniculatus subsp. corniculatus	grote brunel	Prunella grandiflora
origanum vulgare	wit vetkruid	sedum album
plantago media	karthuizer anjer	dianthus carthusianorum
prunella vulgaris	schapengras (fijnbladig)	festuca ovina
rumex acetosella	muizenoor	hieracium pilosella
sedum acre	prachtanjer	Dianthus superbus
sedum album	gewone brunel	prunella vulgaris
sedum rupestre	roze vetkruid	Sedum spurium
silene vulgaris		
thymus pulegioides		
trifolium arvense		

Appendix C: Soil water content

Results

The soil water content is calculated from the permittivity values that are measured (see Figure C1)**.** The moisture contents are in agreement with the porosity of 64% for the substrate, but the field capacity is greater than the field capacity of 21% given by Optigreen (Optigrün, 2013).

The setups show a fast increase of the soil moisture content during rain events and during periods of drought, the soil moisture content decreases over time. The rate of decrease differs between the setups. Setup two shows a steep slope when a dry period kicks off that flattens with decreasing soil moisture content. Setup one and three decrease gradually. The third setup shows more change in soil moisture content compared to the first setup. The first setup contains controversial data that starts in September, showing a decrease in soil moisture content while setup two and three show a fast increase.

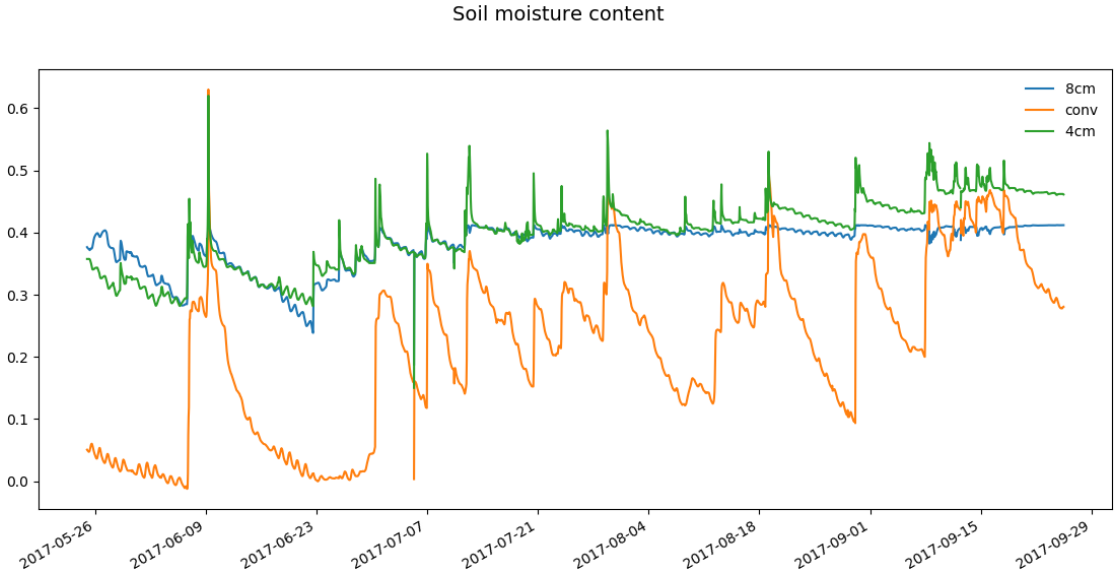

Figure C1 Soil water content measurements

Discussion

The second set up has an expected pattern. During wet periods, the substrate is filled with water, increasing the soil water content. During a dry period, soil water content decreases rapidly the first two days. After, it decreases gradually until there is no moisture left in the soil. The fast decrease of water is caused by evaporation of the soil and transpiration by plants. The gradual decrease with low moisture content is caused by the soil evaporation. The second setup has only sedums growing on the substrate. While soil moisture content decreases, sedums change their metabolic pathway, undergoing the change from C3 to CAM when water becomes limited (Cushman & Borland, 2002).

The pattern for setup one and three is the same as setup two (note that the change is less). The water buffer provides water to the substrate causing an abundant of water (for a long period) for the vegetation on top. The soil moisture content gradually decreases, due to evapotranspiration, and is able to keep the C3 metabolic pathway.

Setup one and three have higher soil moisture contents than expected. The soil moisture contents went to 40% after a wet period, while 21% is expected to be held by the substrate. The higher values for soil moisture content could be related to the presence of the geowicking textile that is ~1 centimetre beneath the sensor. The textile is believed to stay saturated and is able to cause an overestimation of the soil moisture content this way.

The correction factor used for calculating the soil moisture content is 1.667 for setup one and 2.5 for setup two and three. The correction factor is based on the amount of data that is measured as air. Overestimation of the correction factor can bring uncertainties. It is seen that an increase of 1.25 to 1.667 as correction factor is a 10% increase of the soil heat flux.

According to the manual of the 5TE sensor, the volume that is measured with the device is greater than the volume of the soil (in height). The 5TE sensor measures five centimetres above and beneath the sensor, but the setups do not have five centimetre soil beneath it. Except for setup one, which has more than five centimetre soil above the sensor. The sensor measures the permittivity of the substrate as an underestimation since the device will measure a lot of open space (air). The correction factor that has been used is 1.25 for setup one and 2.5 for setup two and three. The corrected soil moisture contents become the measured permittivity times the corrected values.

Appendix D: Linear regressions setup 1 during day time.

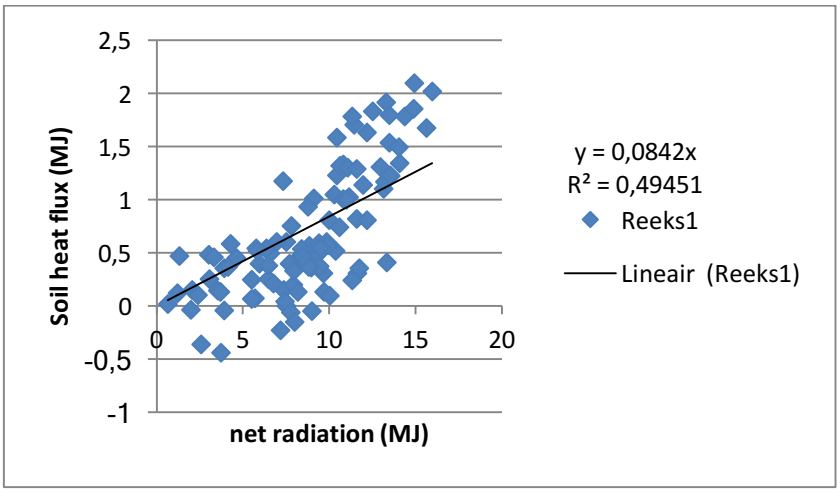

Figure D1 Linear regression of net radiation vs. soil heat flux.

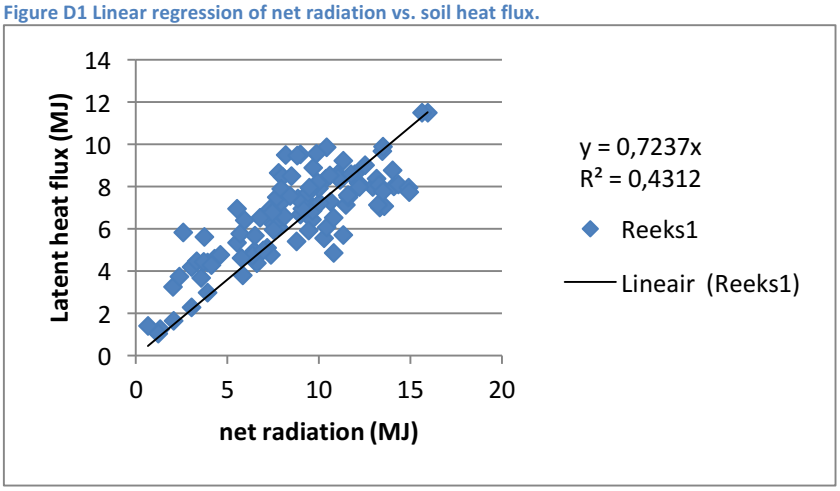

Figure D2 Linear regression of net radiation vs. latent heat flux.

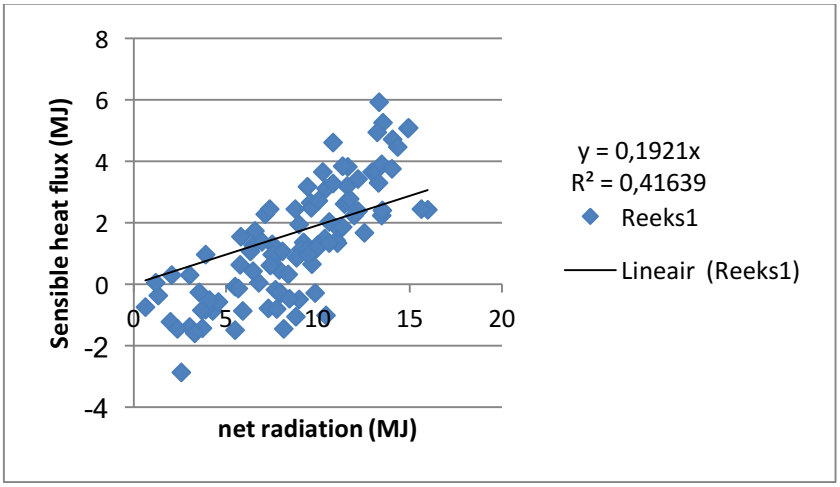

Figure D3 Linear regression of net radiation vs. sensible heat flux.

Appendix E: Linear regressions setup 2 during day time.

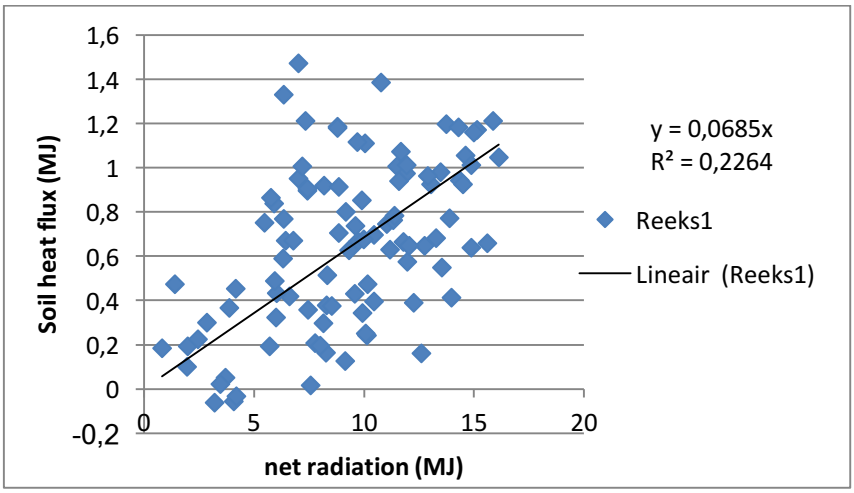

Figure E1 Linear regression of net radiation vs. soil heat flux.

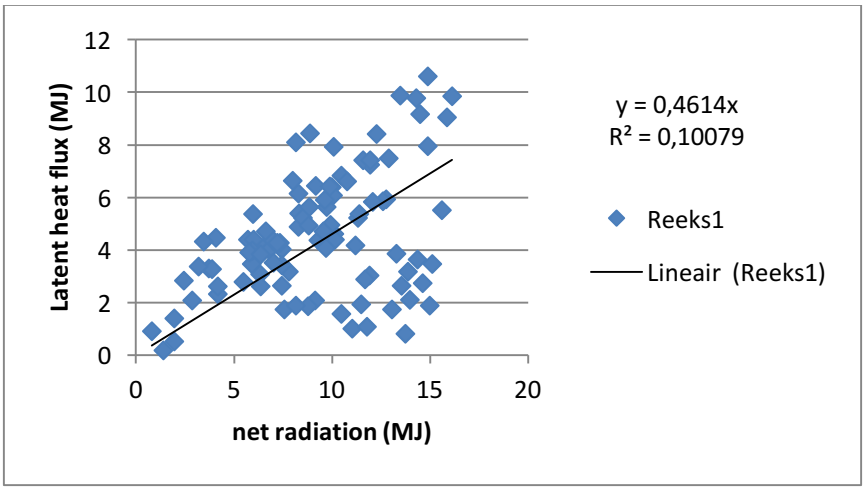

Figure E2 Linear regression of net radiation vs. latent heat flux.

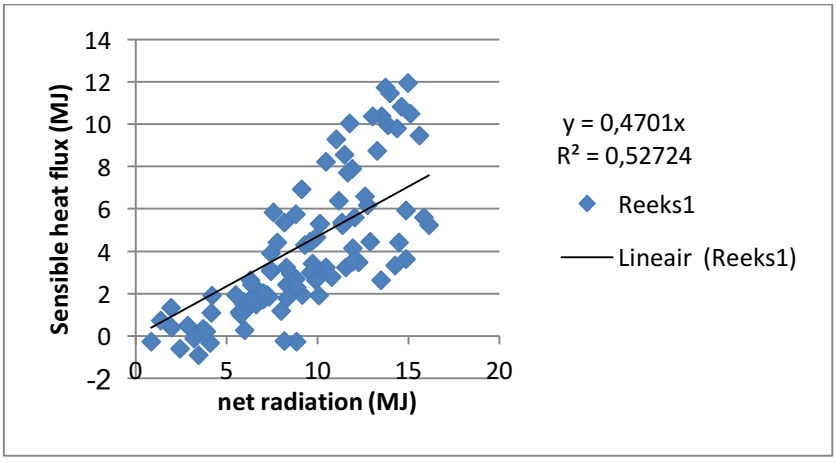

Figure E3 Linear regression of net radiation vs. sensible heat flux.

Appendix F: Linear regressions setup 3 during day time.

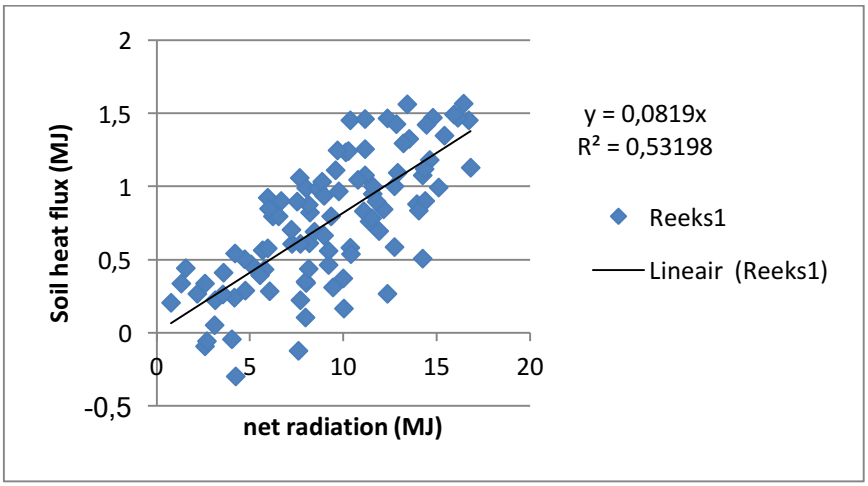

Figure F1 Linear regression of net radiation vs. soil heat flux.

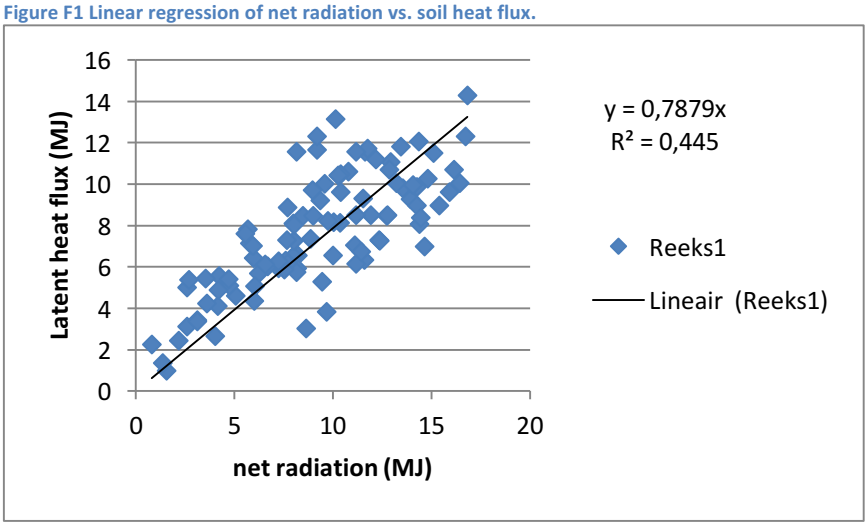

Figure F2 Linear regression of net radiation vs. latent heat flux.

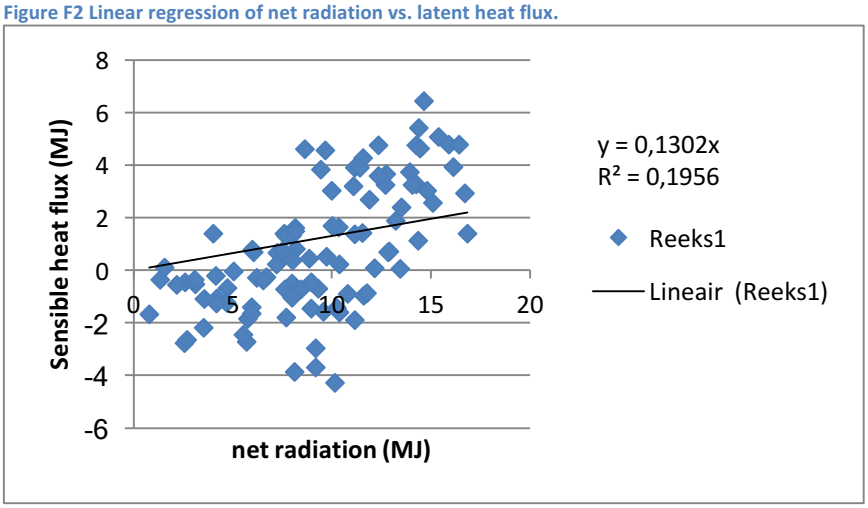

Figure F3 Linear regression of net radiation vs. sensible heat flux.

Appendix G: Hydrus model

The Hydrus model is made for understanding the processes that occur inside the green roof equipped with a storage system. The geometry of the model is two-dimensional axisymmetric (general) and the dimensions are in cm. One capillary cone for the model is considered. The horizontal distance is half the distance of two cones, because this is the maximum lateral distribution.

The properties of the materials are given in Table G1 and their distribution is shown in figure G2. The properties of the Geowicking textile and the capillary cones are derived from retention curves, because they are unknown. Next to that, we considered time variable boundary conditions, single porosity according Genuchten-Mualem and no hysteresis. We applied three boundary conditions: an atmospheric boundary on top of the system, a seepage flux on top of the storage and no flux on all other boundaries. The climatic data from the green roof is applied, which provides insight in the behaviour of the water content in the system (see Figure G1).

Simulations show that during dry days, when evaporation occurs, the water content of the soil decreases. Whereas the substrate and the storage decrease rapidly, the geowicking textile and the capillary cones decrease slowly. During precipitation, the water content of the substrate and the storage increases rapidly.

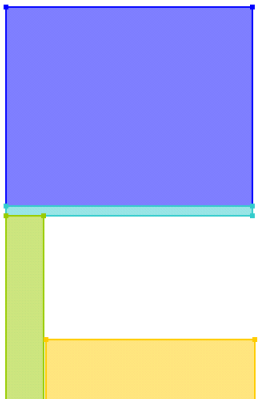

Figure G2 Schematic figure of setup one. From top to bottom: Substrate is blue, geowicking textile is cyan, capillary cone is green and the storage filled with water is yellow.

Table G1 Properties of the used materials.

Mat	Name	Qr [-]	Qs [-]	Alpha [1/cm]	n [-]	Ks [cm/day]	l [-]
1	Substrate	0,02	0,64	0,145	3	2000	0,5
2	Geowicking textile	0,01	0,55	0,05	1,5	4000	0,5
3	Capillary cone	0,015	0,48	0,05	1,7	2500	0,5
4	Water	0,001	0,95	0,2	20	5000	-0,5

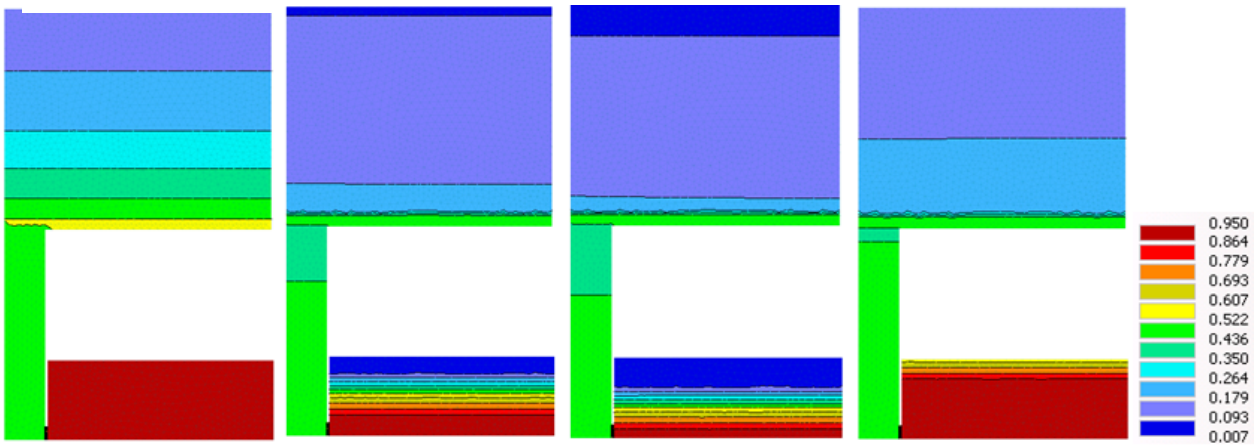

Figure G1 From left to right: 1. Are the initial conditions in equilibrium, 2. Is the state after 5 days with evaporation, 3. Is the state after 7 days with evaporation and 4. Is the state of day 9, which had two days of precipitation. The legend on the right gives the colours and the according water content value.